PCCP

ROYAL SOCIETY OF CHEMISTRY

PAPER

View Article Online
View Journal | View Issue

Cite this: *Phys. Chem. Chem. Phys.*, 2025, **27**, 24256

Structure, spectra, and intracluster chemistry of gas-phase platinum nitrosyl ion–molecule complexes

Philip A. J. Pearcy, Edward I. Brewer, Gabriele Meizyte, Scott Harrington, Matthew Doll, Peter D. Watson, † Christian T. Haakansson and Stuart R. Mackenzie *

Received 8th September 2025,
Accepted 15th October 2025

DOI: 10.1039/d5cp03460d

rsc.li/pccp

The structures of gas-phase platinum nitrosyl ion–molecule complexes, $[Pt(NO)_n]^+$ (n = 3–7), have been investigated using a combination of infrared photodissociation action spectroscopy and quantum chemical simulations. Nitric oxide binds in a combination of linear and bent motifs associated with nominal three- and one-electron donation, respectively, and there is clear evidence of a first solvation shell closing at six ligands. Oxygen rich complexes are also observed in the mass spectrum and their infrared spectra indicate the formation of an N_2O_3 moiety. Calculations support the interpretation of $[Pt(N_2O_3)(NO)_n]^+$ complexes arising from exothermic intracluster reactions in which $[\cdots(NO)_3\cdots]^+$ complexes form $[\cdots(NO_2)(N_2O)\cdots]^+$ species from which the more weakly-bound nitrous oxide is lost.

1. Introduction

Nitrogen oxides (NO_x) play important roles in human health as well as the wider environment.[1–4] The simplest, the stable radical nitric oxide (NO, $X\,^2\Pi$) is involved in many physiological processes as a messenger molecule in mammalian bodies.[5] It is also a well-known pollutant gas produced both anthropogenically, in combustion and agricultural processes,[6] and naturally, such as in lightning strikes.[7] Common strategies to lower NO_x levels involve passing exhaust gases over finely dispersed transition metals which catalyse their reduction to harmless molecules.

Platinum is an element synonymous with both heterogeneous and homogeneous catalysts. NO reduction has been studied extensively both in electrochemical cells[8] and on extended surfaces,[9–12] where reversible oxide formation occurs.[13] Investigation of the fundamental interaction of NO with platinum-containing active sites offers the potential for a better understanding of the catalytic process.

Gas-phase clusters and ion–molecule complexes offer experimentally and theoretically tractable model systems for studying molecular activation at metal centres, providing key insights into catalytically active sites[14,15] as well as intracluster chemistry.[16–18] Extensive spectroscopic and/or reactivity studies of NO with gas-phase metal centres have been reported including clusters of cobalt[19–26] and nickel,[27–29] as well as precious metals such as rhodium,[30–34] silver,[35] iridium,[36] and gold.[37,38] As befits the extensive catalytic use of platinum, the properties of $Pt_n^{+/0/-}$ and $Pt_nO_x^{+/0/-}$ clusters have been studied extensively,[39,40] as well as their reactions with small molecules,[41–54] including nitric oxide.[55]

Bohme *et al.* performed a comprehensive study on NO reactivity with metal cations in selective ion flow tube (SIFT) reactions[56] and determined that the main products of termolecular Pt^+ + NO + NO reactions were $PtNO^+$ (10%) and PtNO (90%, in conjunction with NO^+) with $PtNO^+$ reacting further to produce $Pt(NO)_{2,3}^+$.

NO binds to cationic centres either linearly or nonlinearly as a three- or one-electron donor, respectively.[57,58] The nature of the binding also affects the NO bond itself, as reflected in its vibrational frequency. Coupled with the open shell nature of NO, this leads to complex potential energy landscapes with large numbers of structural isomers which present a severe challenge for quantum chemical calculations, such as density functional theory (DFT) calculations.[59]

Infrared photodissociation (IRPD) provides a direct spectroscopic measure of molecular activation and IRPD studies of transition metal nitrosyl ion–molecule complexes, $[M(NO)_n]^+$, were pioneered by Zhou *et al.* for Fe^+, Cu^+, Ag^+ and Au^+.[60–62] They observed the formation of NO dimers following the closing of the first solvation shell, illustrated by the emergence of new satellite bands in the infrared action spectrum. The number of NO molecules in the first coordination shell varies: 4 for Fe^+ and Cu^+, 5 for Ag^+, and 2 for Au^+. We have previously reported the spectra of nitrosyl complexes of Group 9 metal

Department of Chemistry, University of Oxford, Chemistry Research Laboratory, Mansfield Road, Oxford, OX1 3TA, UK. E-mail: stuart.mackenzie@chem.ox.ac.uk
† Current address: Western Australian School of Mines: Minerals, Energy and Chemical Engineering, Curtin University, Bentley, Australia, 6102.

cations[63] with Co^+ and Ir^+ behaving similarly to Fe^+ and Cu^+ but more complex spectra were obtained for $Rh(NO)_n^+$.

Here, we present IRPD studies of NO complexes with Pt^+, $[Pt(NO)_n]^+$ (n = 3–7), with spectra interpreted with the help of DFT calculations. We continue to apply our square bracket nomenclature (*i.e.*, $[Pt(NO)_n]^+$) to indicate that species are assigned initially on the basis of their mass, with spectroscopy providing structural information.

2. Experimental and computational methods

Our experimental instrument has been previously detailed.[64–67] In brief, a rotating Pt disk target is ablated at 20 Hz within a cutaway source[68] using a focused 532 nm pulse from a Nd:YAG laser (8 ns pulse, 2–10 mJ per pulse as necessary). Ablation takes place in the throat of a pulsed supersonic expansion of a carrier gas seeded with NO (~2% in Ar for $[Pt(NO)_n]^+$, 5% in He for $[PtO(NO)_n]^+$), no purification of the NO gas was completed. The resulting molecular beam is skimmed before ions are mass-selected in a quadrupole mass filter/quadrupole bender arrangement. Cationic species are extracted orthogonally into a reflectron time-of-flight (ReToF) mass spectrometer for detection.

IRPD spectra are recorded by intersecting alternate pulses of the cluster beam with counter-propagating, tunable, infrared pulses from a tabletop optical parametric oscillator/optical parametric amplifier (OPO/OPA, Laservision), operating in the 1500–2100 cm^{-1} region. Spectra of mass-selected parent complexes are recorded as a function of wavenumber in the daughter fragment channels against a zero background. IRPD spectra are reported as absorption cross-sections, σ, using a modified Beer–Lambert law:[69]

$$\sigma = -\frac{1}{\Phi}\ln\left(1 - \frac{N_f}{\alpha N_0}\right), \quad (1)$$

where Φ is the photon flux and N_f and N_0 are the intensities of the fragment and parent ion signals, respectively. α is a scaling factor describing the overlap of the molecular beam and the infrared beam, and it is assumed to be unity. For simplicity, only the data for complexes containing the three most abundant Pt isotopes (^{194}Pt, ^{195}Pt, and ^{196}Pt)[70] are used. Spectra of individual isotopologues are compared with those of the ^{195}Pt isotopologue (with odd mass) before being included in the averaging to avoid accidental contamination from isobaric species including pure $[(NO)_n]^+$ or $[O_x(NO)_n]^+$ complexes.[67]

Assignment of experimental spectra is performed with the help of spectra simulated for energetically low-lying structures computed using DFT. Calculated structures are produced using the Gaussian 16 software package[71] with a stochastic conformer search completed based on starting structures generated using a modified Kick[3] algorithm.[72] Open-shell NO ($^2\Pi$) and Pt^+ (^2D ground state) represent particular difficulties for DFT,[59] leading to multiple low-lying electronic states and isomeric forms of $[Pt(NO)_n]^+$. We employ a B3P86/def2TZVP[73–76] level of theory which has been shown to perform well in previous studies.[77,78] All calculations presented are for the ^{195}Pt isotope. A scaling factor of 0.9347 is applied to computed harmonic vibrational frequencies of the nitrosyl complexes based on the calculated frequency of the 'free' NO stretch (1875.84 cm^{-1}).[79,80] All calculated energies reported here are zero-point corrected and calculated line spectra are convoluted with Lorentzian line shapes (8 cm^{-1} full width half maximum) for comparison with experimental data. Based on previous work,[67] additional calculations were performed for $[PtO(NO)_n]^+$ and $[Pt(NO_2)(NO)_{n-1}]^+$ structures. Bond dissociation energies (BDEs) are calculated from zero-point corrected energies for the respective ground state parent and fragment species as follows:

$$BDE = E\left(\left[PtO_x(NO)_{n-1}\right]^+\right) + E(NO) - E\left(\left[PtO_x(NO)_n\right]^+\right) \quad (2)$$

3. Results and discussion

3.1. Time-of-flight mass spectrum of $[PtO_x(NO)_n]^+$

Fig. 1 shows a typical mass spectrum recorded using a 2% NO in Ar gas mixture. The mass spectrum is dominated by $[Pt(NO)_n]^+$ and $[PtO(NO)_n]^+$ complexes, clearly identifiable by the distinctive Pt isotope distribution (*ca.* 1 : 1 : 1 : 0.25 for ^{194}Pt : ^{195}Pt : ^{196}Pt : ^{198}Pt).[70] The intensities of the $[Pt(NO)_n]^+$ species appear to follow a simple Poisson distribution peaking at n = 2. The ion signals for the $[PtO(NO)_n]^+$ (n = 1, 2) appear anomalously weak and the $[PtO(NO)_3]^+$ species are pronounced.

The origin of the $[PtO(NO)_n]^+$ species is uncertain. Importantly, they do not arise from NO binding to PtO^+ since no oxide peaks are observed when the Pt target is ablated in pure Ar (see Fig. S1, SI). Similarly, in SIFT studies of Pt^+ + NO reactions, Bohme *et al.* found NO^+ and $[Pt(NO)_{1-3}]^+$ products, but no oxides.[56] Furthermore, Armentrout *et al.* showed that, under single collision conditions, PtO^+ + NO reactions yield Pt^+, $[Pt(NO)]^+$, and NO^+ products, with the charge transfer reaction the most efficient at low collision energies.[81] Based on the relative ion signals in the mass spectrum and evidence in the infrared spectra discussed later, we believe that the oxygen rich $[PtO(NO)_n]^+$ complexes are produced in intra-cluster reactions within $[Pt(NO)_n]^+$ resulting in nitrous oxide loss:

$$\left[Pt(NO)_n\right]^+ + NO \rightarrow [PtO(NO)_{n-1}(N_2O)]^+ \rightarrow \left[PtO(NO)_{n-1}\right]^+ + N_2O \quad (3)$$

$$\left[Pt(NO)_n\right]^+ + NO \rightarrow [Pt(NO_2)(NO)_{n-2}(N_2O)]^+ \rightarrow \left[Pt(NO_2)(NO)_{n-2}\right]^+ + N_2O \quad (4)$$

We cannot, however, rule out the possibility that the ablation laser is involved in a photochemical step.[82] We have previously reported spectroscopic evidence for analogous reactions occurring in pure gas-phase $(NO)_n^+$ clusters.[67]

The mass spectra show clear evidence of pure nitrogen and oxygen – containing clusters, separated by 76 u (= N_2O_3) which we assign as $[(NO)_{1,3}(N_2O_3)_n]^+$ complexes,[82] arising from NO intracluster reactions in complexes nucleating around NO^+.[67]

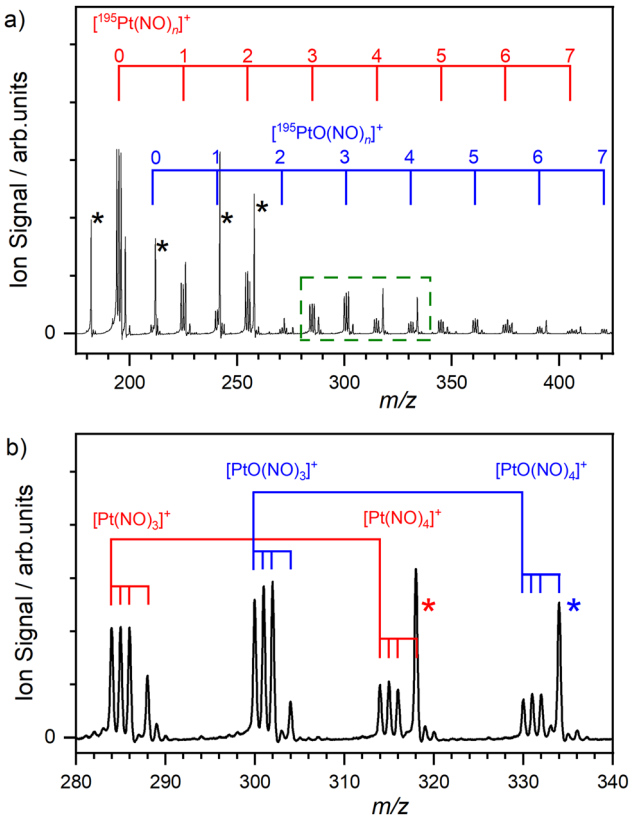

Fig. 1 (a) Time-of-flight mass spectrum of species produced upon ablation of a Pt target in the presence of a 2% NO in Ar (6 bar backing pressure). (b) Expanded 280 ≤ m/z ≤ 340 region of the mass spectrum in which the four most abundant Pt isotopes are clearly resolved. Asterisks indicate blended peaks contaminated by pure N, O complexes, specifically $[(NO)_3(N_2O_3)_3]^+$ (red) and $[(NO)(N_2O_3)_4]^+$ (blue).

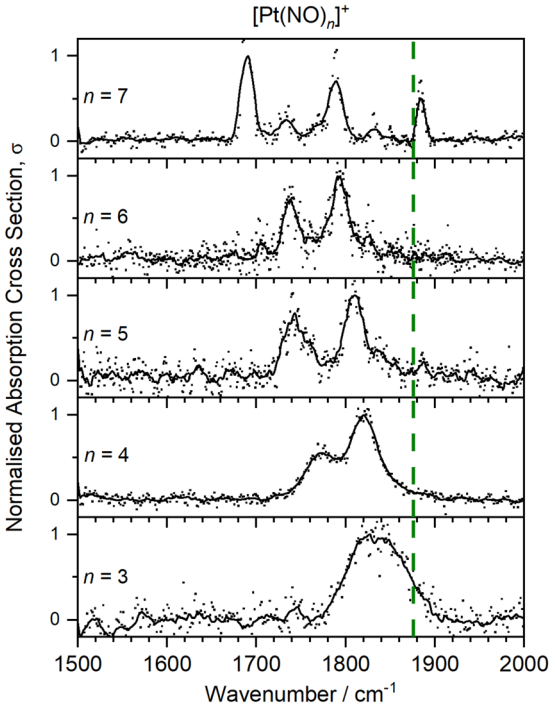

Fig. 2 IRPD spectra of the $[Pt(NO)_n]^+$ complexes (n = 3–7), measured in the enhancement of the $[Pt(NO)_{n-1}]^+$ daughter fragment channel, and presented as normalised absorption cross sections for each value of n. The green dashed line indicates the free NO stretch at 1875.84 cm^{-1}.[79,80]

The dinitrogen trioxide, N_2O_3, arises from intermolecular bonding of NO and NO_2 radicals to form a stable singlet. Some of these species are isobaric with $[^{198}PtO_x(NO)_n]^+$ complexes, as shown in Fig. 1 and care has been taken to exclude them from the spectra reported here.

3.2. Infrared action spectra of $[Pt(NO)_n]^+$ ion–molecule complexes

3.2.1. Overview. The infrared action (IRPD) spectra of $[Pt(NO)_n]^+$ complexes (n = 3–7) between 1500–2000 cm^{-1} are shown in Fig. 2. The only fragmentation pathway observed is loss of NO, and the spectra shown are recorded in enhancement of the $[Pt(NO)_{n-1}]^+$ daughter. Fig. S2 (SI) shows how the fitted peak positions change as a function of complex size, n.

No dissociation was observed for $[Pt(NO)_n]^+$ n = 1, 2 and hence no spectra are shown. This occurs in IRPD studies when the ligand binding energy significantly exceeds the photon energy. The calculated bond dissociation energies (BDE) for n = 1, 2 are calculated to be 4.63 and 2.00 eV, respectively representing approximately 20 and 9 photons, respectively. Fig. S10 shows the BDEs for the $[Pt(NO)_n]^+$ complexes considered here.

The smallest complex for which a spectrum was obtained was $[Pt(NO)_3]^+$. The comparatively poor signal-to-noise ratio (SNR) and the broad, unresolved spectral peak shown in the spectrum suggest multiple photon absorption.

The main trends observed in the $[Pt(NO)_n]^+$ data from n = 3 to n = 6 include a progressive redshift of the spectrum away from the free NO stretch at 1875.84 cm^{-1} coupled with the observation of more, better resolved spectral features whose spacing increases with n. In all of these trends, the $[Pt(NO)_n]^+$ spectra show marked similarity with the spectra of $[Rh(NO)_n]^+$.[63] Evidence of satellite bands (to the red and the blue of the main cluster of bands) assigned as NO-dimer bands in other $[M(NO)_n]^+$ ($n \geq 5$) systems are less pronounced in the present case,[61,63] with these satellite bands not observed until n = 7 in the present study. The SNR of the n = 5, 6 species is poorer than seen in previous studies, suggesting alternative structural motifs with no secondary solvation shell formed.

For n = 7, by contrast, the spectrum is better resolved, and the SNR is much improved. The spectrum can be understood as a continuation of the trend for the two main spectral features observed for the smaller species, with additional bands appearing at 1691 cm^{-1} and 1885 cm^{-1}, respectively. Based on previous studies, we interpret these additional bands as NO molecules binding in a secondary solvation shell as a dimer motif with one of the first shell ligands. This suggests that Pt^+ can accommodate up to six NO molecules in the first coordination shell.

Charge–dipole interactions dominate the electrostatic interactions of NO binding to metal centres, resulting in polarisation of the NO bond and increased IR activity. More chemical bonding arises *via* (a) σ–donation of an NO lone pair,

(b) π–donation from the unpaired NO π* electron, and (c) π-backbonding from occupied d-orbitals on the metal centre to the NO π* orbital (expected to be negligible in bonding to a metal cation). Hence, NO can act as either a (π*) one-electron donor, producing nonlinear M^+–N=O coordination, or as a ($\pi^*\sigma^2$) three-electron donor which leads to linear M^+–N≡O structures.[2]

3.2.2. Structural assignments. Fig. 3 compares the experimental IRPD spectra of (a) $[Pt(NO)_3]^+$ and (b) $[Pt(NO)_4]^+$ with simulated IR spectra of the calculated structure that best fits the experimental data. Other simulated spectra are provided in the SI (Section S4 and Fig. S3, S4, S6 and S8). For n = 3, the simulated spectrum for the lowest energy isomer, Isomer 3a, is in good agreement with the unresolved spectral band. This structure, a triplet state, is a near planar complex, with two NO molecules binding linearly (as three-electron donors) and the third in a bent fashion (a one-electron donor). Binding to a Pt^+ ion ($[Xe]4f^{14}5d^9$), this results in a stable 16-electron system, not uncommon for planar Pt(I) complexes.[83] The two bands in the simulated spectrum at 1818 cm^{-1} and 1850 cm^{-1} are IR-active normal modes involving all three NO molecules. The 1818 cm^{-1} mode involves a larger contribution from the bent NO molecule, the mode at 1850 cm^{-1} an out-of-phase vibration of the two linearly-bound NO ligands. Other, higher energy structures involving either dimer moieties, singlet multiplicities, or O-bound NO molecules present poor comparison with the experimental spectrum.

For $[Pt(NO)_4]^+$, Isomer 4c ($2S$ + 1 = 4) best replicates the experimental spectrum. Near-square-planar, Isomer 4c lies 0.04 eV higher than the lowest energy structure, Isomer 4a (see Section S2a, SI). All four NO ligands bind nonlinearly to the Pt^+ ion. As shown in Fig. 3b, the main bands seen in the experimental spectrum comprise three distinct modes which are not fully resolved. A very weak fourth vibration at 1871 cm^{-1} (corresponding to the "breathing" motion) is not discernable in the experimental spectrum. Consistent with the experimental spectrum, the IR active modes are slightly redshifted compared to the n = 3 spectrum, suggesting slightly stronger activation of the NO. The same trend was observed for $[Rh(NO)_n]^+$.[63]

Comparisons of experimental and simulated spectra were also performed for the larger complexes (n = 5–7) as shown in Fig. 4. As seen from the convincing simulations in Fig. 4a and b, platinum nitrosyl complexes adopt a square-based pyramidal structure for n = 5, and an octahedral structure for n = 6. Isomer 5c ($2S$ + 1 = 3, E = 0.06 eV) builds upon the structure of Isomer 4c by having a base with four bent NO molecules bound to the Pt^+ centre, with a fifth NO bound to the top site. The experimental and simulated spectra are in good agreement, with two main bands centered at 1743 cm^{-1} and 1810 cm^{-1}. The 1810 cm^{-1} band is multiple unresolved modes; all different combinations of the NO molecules vibrating either in- or out-of-phase. Additionally, the weak "breathing" mode at 1863 cm^{-1} (simulated) and 1887 cm^{-1} (experiment, possibly) further supports the square-based pyramid assignment.

Addition of a further NO ligand completes the octahedral structure for $[Pt(NO)_6]^+$ (Isomer 6c, $2S$ + 1 = 2, E = 0.02 eV), with all six of the NO molecules bound nonlinearly. All NO bond lengths and bond angles within the complex are very similar in Isomer 6c. Again, there is convincing agreement between the experimental and simulated spectra with two main (unresolved) bands slightly red-shifted from those in the n = 5 spectra. There is no obvious sign of satellite bands arising from NO dimer moieties. The near perfect octahedral symmetry means that the breathing mode (1863 cm^{-1}) is essentially IR inactive. The octahedral structure has not been observed previously in $M^+(NO)_n$ ion–molecule systems and clearly represents a full coordination shell.

The additional NO ligand in $[Pt(NO)_7]^+$ must bind (more weakly) in a second solvation shell giving rise to multiple

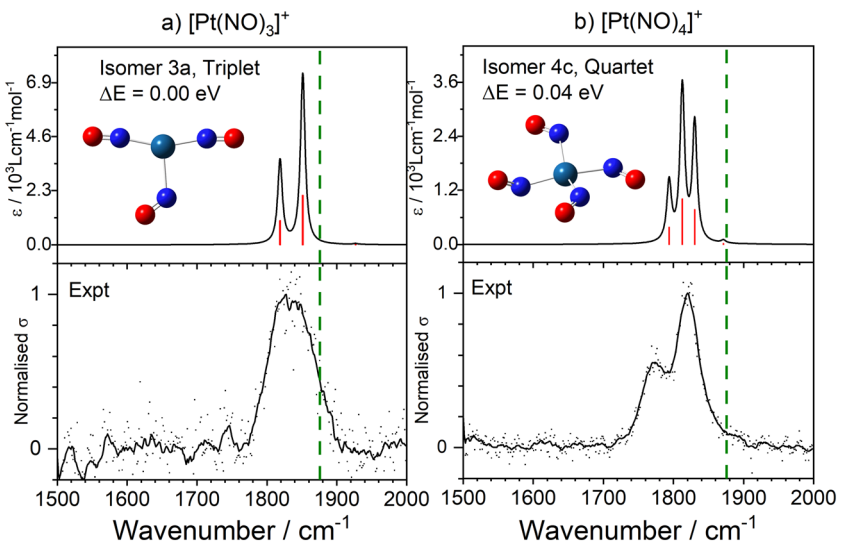

Fig. 3 Experimental IRPD spectra (bottom panels), along with the simulated IR spectra and structures (top panel) for the best-fit low-lying isomers for (a) $[Pt(NO)_3]^+$, and (b) $[Pt(NO)_4]^+$. The green dashed line indicates the free NO stretch at 1875.84 cm^{-1}.[79,80]

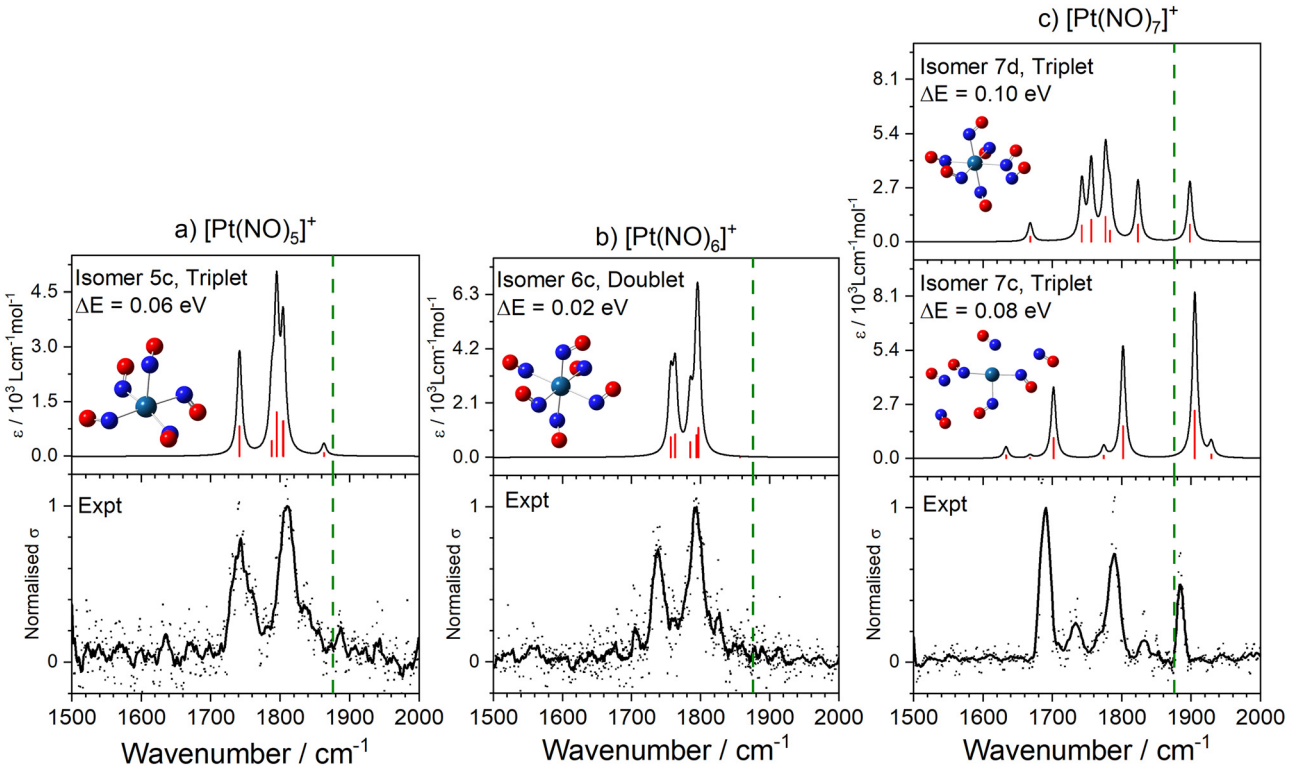

Fig. 4 Experimental IRPD spectra (bottom panels) along with the simulated IR spectra and structures (top panels) for the best-fit low-lying isomers for (a) $[Pt(NO)_5]^+$, (b) $[Pt(NO)_6]^+$, and (c) $[Pt(NO)_7]^+$. The green dashed lines indicate the free NO stretch at 1875.84 cm^{-1}.[79,80]

near-isoenergetic structures. The experimental spectrum marks a clear discontinuity with preceding cluster sizes, with intense bands at the extreme red and blue ends of the spectrum – the latter the first band blue-shifted compared with the free NO stretch. The most convincing fits are provided by Isomers 7c and 7d (both $2S + 1 = 3$), whose spectral features most closely align with those observed. Nevertheless, they are markedly different structures. Isomer 7c has a square-planar core, with one NO dimer and one NO trimer moiety. Its simulated spectrum reproduces the three intense bands, and some intervening weaker features, observed in the IRPD spectrum, albeit with differing relative line strengths. The strong bands arise from modes that mostly contain vibrations associated with the NO dimer and trimer moieties. Isomer 7d is an octahedral structure, with the seventh NO forming a dimer with a first solvation shell ligand. In both structures the ''breathing'' mode is much more intense than for the smaller clusters due to the symmetry breaking provided by the seventh NO. There seems to be stronger evidence for the presence of Isomer 7c but we cannot rule out that both are present in the beam.

3.3. Infrared action spectra of $[PtO(NO)_n]^+$ ion–molecule complexes

3.3.1. Overview. Fig. 5 shows the IRPD spectra of $[PtO(NO)_n]^+$ (n = 4–7) recorded in the 1500–2100 cm^{-1} range. No dissociation was observed for n = 1–3, again presumably due to prohibitively high ligand binding energies. BDEs for the lowest energy calculated structures of the n = 1, 2, and 3 complexes are 2.48 eV, 2.70 eV, and 1.28 eV, respectively (see SI Section S2a). NO loss was again the only fragmentation pathway observed for any of these species.

There are noticeable differences between the spectra of the $[PtO(NO)_n]^+$ complexes (Fig. 5) and those of the simple $[Pt(NO)_n]^+$ species (Fig. 2). In particular, the $[PtO(NO)_n]^+$ spectra exhibit an intense new band markedly blue-shifted with respect to the free NO stretch. The appearance of additional blue-shifted bands in O-rich complexes mirrors our observations in pure $[(NO)_n]^+$ and $[O(NO)_n]^+$ (assigned to $[(NO_2)(NO)_n]^+$) complexes.[67] In $[(NO_2)(NO)_n]^+$ structures, the additional spectral feature is not due to explicit $NO_2^{(+)}$ vibrations as might be suspected, but rather from NO modes whose oscillator strength is greatly increased by interaction with the NO_2 moiety. In the spectra of $[PtO(NO)_n]^+$ complexes here (Fig. 5), the highest wavenumber band redshifts systematically towards 1876 cm^{-1} of the free NO stretch with increasing n. As with the $[Pt(NO)_n]^+$ complexes, the spectra become better resolved with increasing complex size, as the lowest ligand binding energy drops.

In the spectrum of the smallest, $[PtO(NO)_4]^+$ complex, four peaks are observed at 1831 cm^{-1}, 1868 cm^{-1} (weak), 1905 cm^{-1} and 1990 cm^{-1}. The spectrum of the $[PtO(NO)_5]^+$ complex is qualitatively similar but both red-shifted and stretched to lower wavenumber. The three main bands appear at 1745 cm^{-1}, 1817 cm^{-1} and 1952 cm^{-1}, respectively, with a weak shoulder appearing at 1706 cm^{-1}. The general trend of spectral red-shift continues for n = 5, 6, suggesting additional NO ligands bind directly to the Pt core. In this size range, unlike in $[Pt(NO)_n]^+$ complexes, there is no indication of additional peaks signifying NO dimer moiety vibrations.

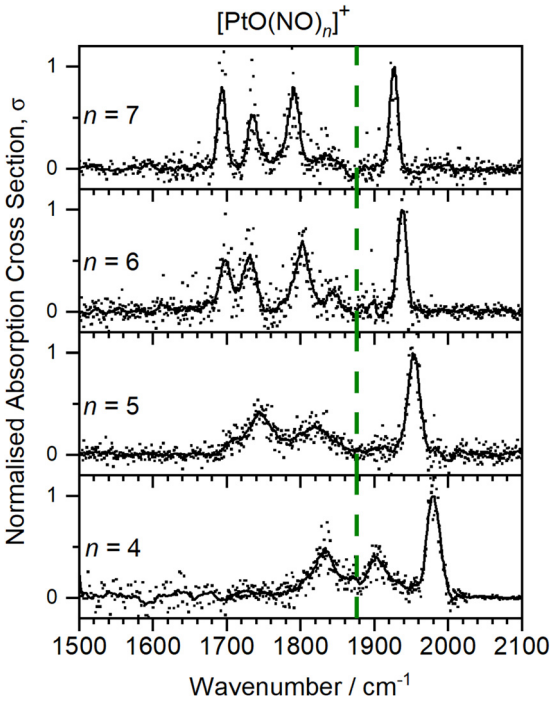

Fig. 5 IRPD spectra of the $[PtO(NO)_n]^+$ complexes (n = 4–7), measured in the enhancement of the $[PtO(NO)_{n-1}]^+$ daughter fragment channel. The green dashed line indicates the free NO stretch at 1875.84 cm^{-1}.[79,80]

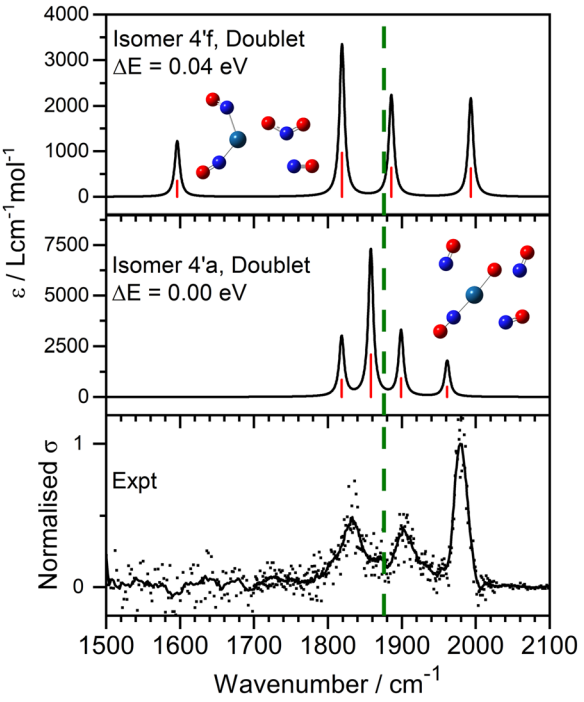

Fig. 6 Experimental IRPD spectra (bottom panel) along with the simulated IR spectra and structures (top panel(s)) for the best-fit low-lying isomers for $[PtO(NO)_4]^+$. The green dashed line indicates the free NO stretch at 1875.84 cm^{-1}.[79,80]

3.3.2. Structural assignments. Fig. 6 shows a comparison of experimental and simulated spectra of the $[PtO(NO)_4]^+$ complex. Among a large number of energetically low-lying isomers (ΔE < 0.1 eV), two distinct calculated structures provide good agreement with the experimental spectrum. The putative ground state, Isomer 4′a (ΔE = 0.00 eV, $2S + 1 = 2$), has a $Pt(NO_2)^+$ core to which three NO molecules are bound directly at the Pt^+ centre, forming a square-planar configuration. The two ligands adjacent to the NO_2 unit bind non-linearly with the remaining NO molecule (opposite the NO_2) linearly bound. The simulated spectrum exhibits peaks in approximately the same positions as those observed experimentally, even if the relative intensities do not match well. The 1961 cm^{-1} band is the symmetric "breathing" motion of all the NO ligands, with oscillator strength dominated by the linearly bound NO opposite the NO_2. The feature at 1818 cm^{-1} arises largely from the vibration of the NO_2 group, with the remaining modes produced from in-phase and out-of-phase vibrations from the nonlinearly bound NO molecules bound *via* the metal centre (see Fig. S7 for vibrational modes).

Isomer 4′f (ΔE = 0.04 eV, $2S + 1 = 2$), by contrast, has only two NO molecules bound to the Pt^+ centre, with the additional NO molecule binding to the Pt-bound NO_2, forming an N_2O_3 moiety. The simulated spectrum reproduces well the three main peak positions in the spectrum (1819 cm^{-1} and 1886 cm^{-1} bands are combined vibrations of the Pt-bound NO molecules, with the 1993 cm^{-1} peak a near local mode in the outer NO ligand in the N_2O_3 unit). The peak in the simulated spectrum around 1590 cm^{-1} is observed neither in this experimental spectrum nor in the spectra of any of the larger complexes. We interpret this as a result of wide amplitude motion in the N_2O_3 moiety which would lead to such a band being considerably broader. Alternatively, the calculated oscillator strength could be systematically overestimated. The NO ligands bound directly to the metal centre have a calculated BDE of 0.41 eV compared with 1.04 eV for the NO in the N_2O_3 moiety, suggesting that it is the loss of these that dominates the IRPD process.

Fig. 7 compares the experimental and simulated spectra of $[PtO(NO)_{5-7}]^+$. For n = 5, two computed structures that produce simulated spectra in good agreement with the experimental peak positions. Both isomers contain an N_2O_3 unit bound as $Pt^+(ONO)(NO)$. The main difference between the two isomers lies in spin multiplicity. The putative ground state, Isomer 5′a is a triplet state, and Isomer 5′b (ΔE = 0.11 eV) is a singlet. Isomer 5′a adopts a square planar configuration, whilst in Isomer 5′b, three NOs form a pseudo-pyramidal structure with Pt^+, with the N_2O_3 unit attaching to the top site. The simulated spectra contain three distinct regions: a weak feature below 1600 cm^{-1} (asymmetric NO_2 stretch), 1700–1875 cm^{-1} (combined NO vibrations) and above 1900 cm^{-1} (NO within the N_2O_3 unit). Both simulated spectra provide good agreement with the experimental spectrum except for the weak band < 1600 cm^{-1} which is not observed at this signal to noise ratio. It could be experimentally broad due to wide amplitude motion or else the simulations overestimate the oscillator strength. The strong feature around 1950 cm^{-1} provides strong evidence of the emergence of the N_2O_3 unit.

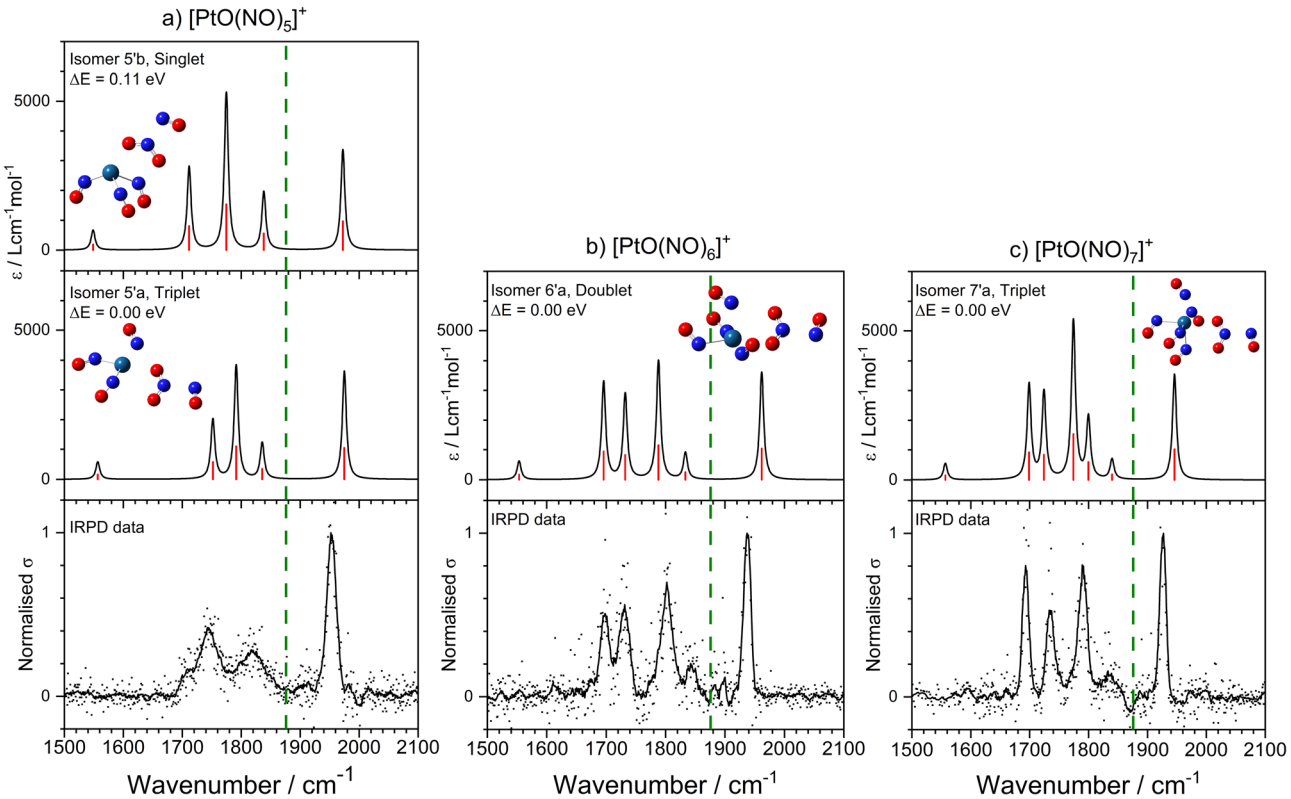

Fig. 7 Experimental IRPD spectra (bottom panels) along with the simulated IR spectra and structures (top panel(s)) for the best-fit low-lying isomers for (a) $[PtO(NO)_5]^+$, (b) $[PtO(NO)_6]^+$, and (c) $[PtO(NO)_7]^+$. The green dashed line indicates the free NO stretch at 1875.84 cm^{-1}.[79,80]

For n = 6 and n = 7, the simulated spectra of the putative ground state structures, Isomer 6′a and Isomer 7′a, agree very well with the experimental data (see Fig. 7b and c). In both cases there is a >0.1 eV gap to the next lowest energy structure. Isomer 6′a adopts a square-based pyramidal structure, with the NO_2 unit of the N_2O_3 in the equatorial plane. Isomer 7′a completes the pseudo-octahedral structure with the seventh NO molecule binding to the Pt centre in the final coordination site. This reflects the structural geometric pattern that was observed for $[Pt(NO)_n]^+$ and suggests $[PtO(NO)_7]^+$ has a filled first coordination shell. It proved impossible to produce enough $[PtO(NO)_8]^+$ to enable a spectrum to be recorded but we would predict the emergence of the $(NO)_2$ dimer as an additional solvation shell is started.

The characteristic N_2O_3 band above 1900 cm^{-1} red shifts smoothly from n = 5 to n = 7 in both the experimental and calculated spectra. This reflects the decreasing charge on the N_2O_3 moiety with increasing NO ligation (see Fig. S11 for calculated Hirshfeld charges). The local NO_2 asymmetric stretch (calculated around 1550 cm^{-1}) is difficult to discern in the experimental spectra and likely suffers from linewidth broadening due to large amplitude motion making it hard to observe. The N_2O_3 moiety itself is surprisingly tightly bound, with the NO BDE ~1 eV for n = 4–7 (Fig. S10). This is significantly larger than the binding energy of NO directly to the Pt^+ centre suggesting that it is the latter that is lost in the IRPD process.

The level of agreement between experimental and simulated spectra is strongly suggestive of $[Pt(N_2O_3)(NO)_n]^+$ structures, providing evidence to suggest the occurrence of intracluster chemistry in the form of $[(NO)_3]^+ \rightarrow [(N_2O)(NO_2)]^+$ (eqn (4)). This reaction is exothermic for $[Pt(NO)_n]$+ where $n \geq 4$ (Section S4, SI), a finding that is consistent with the observations here. Effectively this suggests that the Pt^+ centre catalyses the NO disproportionation reaction.

4. Conclusions

Infrared photodissociation action spectra of $[Pt(NO)_n]^+$ ion–molecule complexes coupled with quantum chemical simulations reveal an initial coordination shell of six in an octahedral arrangement with subsequent NO ligands binding in a second shell *via* formation of the $(NO)_2$ dimer. Individual NO ligands bind as one or three electron donors in bent or linear motifs, respectively, with evidence of 16 and 18 electron complexes. Despite the complexity associated with open shell ligands, the agreement between experiment and simulation is good, providing a high level of confidence in most of the assignments made.

We observe evidence for intracluster reactivity leading to unusual structural moieties and features. Complexes with multiple NO ligands undergo intracluster chemistry forming $[(N_2O)(NO_2)]^+$ structures from which the nitrous oxide (N_2O) is often lost producing $[Pt(NO_2)(NO)_n]^+$ species with characteristic

N_2O_3 (= $(NO_2)(NO)$) moieties. Calculations show that this chemistry becomes energetically feasible once four nitric oxide ligands are bound. The resulting infrared photodissociation action spectra of these species show NO_2 displacing an NO in the inner coordination shell. The formation of an N_2O_3 moiety is strongly supported by observation of a characteristic intense IR peak above 1900 cm^{-1} for each complex size investigated.

Author contributions

The manuscript was written through contributions from all authors. All authors have given approval to the final version of the manuscript.

Conflicts of interest

The authors declare no competing financial interests.

Data availability

Experimental data supporting this article are available from the Oxford Research Archive (DOI: https://dx.doi.org/10.5287/ora-xmzx08j5z).

Supplementary information (SI): computational data supporting this article, as well as additional data interpretation figures. See DOI: https://doi.org/10.1039/d5cp03460d.

Acknowledgements

EPSRC Programme Grant: EP/T021675. This work was supported by EPSRC under Programme Grant EP/T021675, New Directions in Molecular Scattering. PDW thanks Magdalen College, Oxford, for his Fellowship by Examination. PAJP, EIB, and GM are grateful to University College, Somerville College, and Worcester College, Oxford, respectively, for their respective graduate funding.

References

1 T. Boningari and P. G. Smirniotis, *Curr. Opin. Chem. Eng.*, 2016, **13**, 133–141.
2 J. A. McCleverty, *Chem. Rev.*, 2004, **104**, 403–418.
3 R. M. Palmer, A. G. Ferrige and S. Moncada, *Nature*, 1987, **327**, 524–526.
4 C. A. Barth, K. D. Mankoff, S. M. Bailey and S. C. Solomon, *J. Geophys. Res.: Space Phys.*, 2003, **108**, 1027.
5 E. E. van Faassen, S. Bahrami, M. Feelisch, N. Hogg, M. Kelm, D. B. Kim-Shapiro, A. V. Kozlov, H. Li, J. O. Lundberg, R. Mason, H. Nohl, T. Rassaf, A. Samouilov, A. Slama-Schwok, S. Shiva, A. F. Vanin, E. Weitzberg, J. Zweier and M. T. Gladwin, *Med. Res. Rev.*, 2009, **29**, 683–741.
6 J. H. Seinfeld and S. N. Pandis, *Atmospheric chemistry and physics: from air pollution to climate change*, John Wiley & Sons, 2016.
7 L. T. Murray, *Curr. Pollut. Rep.*, 2016, **2**, 115–133.
8 A. C. A. de Vooys, M. T. M. Koper, R. A. van Santen and J. A. R. van Veen, *Electrochim. Acta*, 2001, **46**, 923–930.
9 Z.-P. Liu, S. J. Jenkins and D. A. King, *J. Am. Chem. Soc.*, 2003, **125**, 14660–14661.
10 K. Otto and H. C. Yao, *J. Catal.*, 1980, **66**, 229–236.
11 T. P. Kobylinski and B. W. Taylor, *J. Catal.*, 1974, **33**, 376–384.
12 Y. Bai and M. Mavrikakis, *J. Phys. Chem. B*, 2018, **122**, 432–443.
13 K. Hauff, U. Tuttlies, G. Eigenberger and U. Nieken, *Appl. Catal., B*, 2012, **123–124**, 107–116.
14 D. K. Böhme and H. Schwarz, *Angew. Chem., Int. Ed.*, 2005, **44**, 2336–2354.
15 S. M. Lang and T. M. Bernhardt, *Phys. Chem. Chem. Phys.*, 2012, **14**, 9255–9269.
16 M. Beyer, U. Achatz, C. Berg, S. Joos, G. Niedner-Schatteburg and V. E. Bondybey, *J. Phys. Chem. A*, 1999, **103**, 671–678.
17 M. Beyer, C. Berg, H. W. Görlitzer, T. Schindler, U. Achatz, G. Albert, G. Niedner-Schatteburg and V. E. Bondybey, *J. Am. Chem. Soc.*, 1996, **118**, 7386–7389.
18 G. Niedner-Schatteburg and V. E. Bondybey, *Chem. Rev.*, 2000, **100**, 4059–4086.
19 M. L. Anderson, A. Lacz, T. Drewello, P. J. Derrick, D. P. Woodruff and S. R. MacKenzie, *J. Chem. Phys.*, 2009, **130**, 064305.
20 T. Hanmura, M. Ichihashi and T. Kondow, *Isr. J. Chem.*, 2007, **47**, 37–42.
21 T. Hanmura, M. Ichihashi, R. Okawa and T. Kondow, *Int. J. Mass Spectrom.*, 2009, **280**, 184–189.
22 T. Hanmura, M. Ichihashi, Y. Watanabe, N. Isomura and T. Kondow, *J. Phys. Chem. A*, 2007, **111**, 422–428.
23 J. J. Klaassen and D. B. Jacobson, *J. Am. Chem. Soc.*, 1988, **110**, 974–976.
24 K. Koyama, S. Kudoh, K. Miyajima and F. Mafuné, *J. Phys. Chem. A*, 2015, **119**, 9573–9580.
25 Y. Xie, F. Dong, S. Heinbuch, J. J. Rocca and E. R. Bernstein, *Phys. Chem. Chem. Phys.*, 2010, **12**, 947–959.
26 P. T. Rubli, C. T. Haakansson, P. A. J. Pearcy, R. G. Spratt, J. M. Bakker, P. D. Watson and S. R. Mackenzie, *J. Phys. Chem. A*, 2025, **129**, 5810–5819.
27 W. D. Vann, R. C. Bell and A. W. Castleman, *J. Phys. Chem. A*, 1999, **103**, 10846–10850.
28 W. D. Vann, R. L. Wagner and A. W. Castleman, *J. Phys. Chem. A*, 1998, **102**, 8804–8811.
29 W. D. Vann, R. L. Wagner and A. W. Castleman, *J. Phys. Chem. A*, 1998, **102**, 1708–1718.
30 M. S. Ford, M. L. Anderson, M. P. Barrow, D. P. Woodruff, T. Drewello, P. J. Derrick and S. R. Mackenzie, *Phys. Chem. Chem. Phys.*, 2005, **7**, 975–980.
31 D. Harding, S. R. Mackenzie and T. R. Walsh, *J. Phys. Chem. B*, 2006, **110**, 18272–18277.
32 Y. Zhang, M. Yamaguchi, K. Kawada, S. Kudoh, O. V. Lushchikova, J. M. Bakker and F. Mafuné, *J. Phys. Chem. A*, 2022, **126**, 36–43.
33 M. L. Anderson, M. S. Ford, P. J. Derrick, T. Drewello, D. Phil Woodruff and S. R. Mackenzie, *J. Phys. Chem. A*, 2006, **110**, 10992–11000.
34 J. M. Bakker and F. Mafuné, *Phys. Chem. Chem. Phys.*, 2022, **24**, 7595–7610.

35 J. Hagen, L. D. Socaciu-Siebert, J. Le Roux, D. Popolan, S. Vajda, T. M. Bernhardt and L. Wöste, *Int. J. Mass Spectrom.*, 2007, **261**, 152–158.
36 M. Yamaguchi, Y. Zhang, O. V. Lushchikova, J. M. Bakker and F. Mafuné, *J. Phys. Chem. A*, 2022, **126**, 6668–6677.
37 A. Fielicke, G. Von Helden, G. Meijer, B. Simard and D. M. Rayner, *Phys. Chem. Chem. Phys.*, 2005, **7**, 3906–3909.
38 M. Yamaguchi, Y. F. Zhang, O. Lushchikova, J. M. Bakker and F. Mafuné, *J. Phys. Chem. A*, 2021, **125**, 9040–9047.
39 C. Kerpal, D. J. Harding, A. C. Hermes, G. Meijer, S. R. Mackenzie and A. Fielicke, *J. Phys. Chem. A*, 2013, **117**, 1233–1239.
40 D. J. Harding, C. Kerpal, D. M. Rayner and A. Fielicke, *J. Chem. Phys.*, 2012, **136**, 211103.
41 U. Achatz, C. Berg, S. Joos, B. S. Fox, M. K. Beyer, G. Niedner-Schatteburg and V. E. Bondybey, *Chem. Phys. Lett.*, 2000, **320**, 53–58.
42 I. Balteanu, O. Petru Balaj, M. K. Beyer and V. E. Bondybey, *Phys. Chem. Chem. Phys.*, 2004, **6**, 2910–2913.
43 M. Brönstrup, D. Schröder, I. Kretzschmar, H. Schwarz and J. N. Harvey, *J. Am. Chem. Soc.*, 2001, **123**, 142–147.
44 A. E. Green, J. Justen, W. Schöllkopf, A. S. Gentleman, A. Fielicke and S. R. Mackenzie, *Angew. Chem., Int. Ed.*, 2018, **57**, 14822–14826.
45 A. C. Hermes, S. M. Hamilton, G. A. Cooper, C. Kerpal, D. J. Harding, G. Meijer, A. Fielicke and S. R. Mackenzie, *Faraday Discuss.*, 2012, **157**, 213–225.
46 E. Hernández, V. Bertin, J. Soto, A. Miralrio and M. Castro, *J. Phys. Chem. A*, 2018, **122**, 2209–2220.
47 C. Kerpal, D. J. Harding, D. M. Rayner and A. Fielicke, *J. Phys. Chem. A*, 2013, **117**, 8230–8237.
48 Y. Shi and K. M. Ervin, *J. Chem. Phys.*, 1998, **108**, 1757–1760.
49 D. Trevor, D. Cox and A. Kaldor, *J. Am. Chem. Soc.*, 1990, **112**, 3742–3749.
50 D. Trevor, R. Whetten, D. Cox and A. Kaldor, *J. Am. Chem. Soc.*, 1985, **107**, 518–519.
51 J. Velasquez and M. A. Duncan, *Chem. Phys. Lett.*, 2008, **461**, 28–32.
52 O. W. Wheeler, M. Salem, A. Gao, J. M. Bakker and P. B. Armentrout, *J. Phys. Chem. A*, 2016, **120**, 6216–6227.
53 H. Yamamoto, K. Miyajima, T. Yasuike and F. Mafuné, *J. Phys. Chem. A*, 2013, **117**, 12175–12183.
54 K. Koszinowski, D. Schröder and H. Schwarz, *J. Phys. Chem. A*, 2003, **107**, 4999–5006.
55 J. Yamagishi, K. Miyajima, S. Kudoh and F. Mafuné, *J. Phys. Chem. Lett.*, 2017, **8**, 2143–2147.
56 V. Blagojevic, E. Flaim, M. J. Y. Jarvis, G. K. Koyanagi and D. K. Bohme, *J. Phys. Chem. A*, 2005, **109**, 11224–11235.
57 J. H. Enemark and R. D. Feltham, *Coord. Chem. Rev.*, 1974, **13**, 339–406.
58 T. W. Hayton, P. Legzdins and W. B. Sharp, *Chem. Rev.*, 2002, **102**, 935–992.
59 J. Gräfenstein and D. Cremer, *Phys. Chem. Chem. Phys.*, 2000, **2**, 2091–2103.
60 Y. Li, L. Wang, H. Qu, G. Wang and M. Zhou, *J. Phys. Chem. A*, 2015, **119**, 3577–3586.
61 L. Wang, G. Wang, H. Qu, H. Li and M. Zhou, *Phys. Chem. Chem. Phys.*, 2014, **16**, 10788–10798.
62 L. Wang, G. Wang, H. Qu, C. Wang and M. Zhou, *J. Phys. Chem. A*, 2014, **118**, 1841–1849.
63 G. Meizyte, P. A. J. Pearcy, P. D. Watson, E. I. Brewer, A. E. Green, M. Doll, O. A. Duda and S. R. Mackenzie, *J. Phys. Chem. A*, 2022, **126**, 9414–9422.
64 A. Iskra, A. S. Gentleman, A. Kartouzian, M. J. Kent, A. P. Sharp and S. R. Mackenzie, *J. Phys. Chem. A*, 2017, **121**, 133–140.
65 A. E. Green, R. H. Brown, G. Meizyte and S. R. Mackenzie, *J. Phys. Chem. A*, 2021, **125**, 7266–7277.
66 P. D. Watson, G. Meizyte, P. A. J. Pearcy, E. I. Brewer, A. E. Green, C. Robertson, M. J. Paterson and S. R. Mackenzie, *Phys. Chem. Chem. Phys.*, 2024, **26**, 16589–16596.
67 P. D. Watson, G. Meizyte, P. A. J. Pearcy, E. I. Brewer, A. E. Green, A. J. Stace and S. R. Mackenzie, *J. Phys. Chem. A*, 2025, **129**, 3867–3875.
68 M. A. Duncan, *Rev. Sci. Instrum.*, 2012, **83**, 41101.
69 C. Walther, S. Becker, G. Dietrich, H. J. Kluge, M. Lindinger, K. Lützenkirchen, L. Schweikhard and J. Ziegler, *Z. Phys. D: At., Mol. Clusters*, 1996, **38**, 51–58.
70 F. G. Kondev, M. Wang, W. J. Huang, S. Naimi and G. Audi, *Chin. Phys. C*, 2021, **45**, 030001.
71 M. J. Frisch, G. W. Trucks, H. B. Schlegel, G. E. Scuseria, M. A. Robb, J. R. Cheeseman, G. Scalmani, V. Barone, G. A. Petersson, H. Nakatsuji, X. Li, M. Caricato, A. V. Marenich, J. Bloino, B. G. Janesko, R. Gomperts, B. Mennucci, H. P. Hratchian, J. V. Ortiz, A. F. Izmaylov, J. L. Sonnenberg Williams, F. Ding, F. Lipparini, F. Egidi, J. Goings, B. Peng, A. Petrone, T. Henderson, D. Ranasinghe, V. G. Zakrzewski, J. Gao, N. Rega, G. Zheng, W. Liang, M. Hada, M. Ehara, K. Toyota, R. Fukuda, J. Hasegawa, M. Ishida, T. Nakajima, Y. Honda, O. Kitao, H. Nakai, T. Vreven, K. Throssell, J. A. MontgomeryJr., J. E. Peralta, F. Ogliaro, M. J. Bearpark, J. J. Heyd, E. N. Brothers, K. N. Kudin, V. N. Staroverov, T. A. Keith, R. Kobayashi, J. Normand, K. Raghavachari, A. P. Rendell, J. C. Burant, S. S. Iyengar, J. Tomasi, M. Cossi, J. M. Millam, M. Klene, C. Adamo, R. Cammi, J. W. Ochterski, R. L. Martin, K. Morokuma, O. Farkas, J. B. Foresman and D. J. Fox, *Gaussian 16 Rev. C.01*, Gaussian, Inc., 2016.
72 M. A. Addicoat and G. F. Metha, *J. Comput. Chem.*, 2009, **30**, 57–64.
73 J. P. Perdew, *Phys. Rev. B: Condens. Matter Mater. Phys.*, 1986, **33**, 8822–8824.
74 F. Weigend, *Phys. Chem. Chem. Phys.*, 2006, **8**, 1057–1065.
75 F. Weigend and R. Ahlrichs, *Phys. Chem. Chem. Phys.*, 2005, **7**, 3297–3305.
76 A. D. Becke, *J. Chem. Phys.*, 1993, **98**, 5648–5652.
77 E. I. Brewer, A. E. Green, A. S. Gentleman, P. W. Beardsmore, P. A. J. Pearcy, G. Meizyte, J. Pickering and S. R. Mackenzie, *Phys. Chem. Chem. Phys.*, 2022, **24**, 22716–22723.
78 G. Meizyte, R. H. Brown, E. I. Brewer, P. D. Watson and S. R. Mackenzie, *J. Phys. Chem. A*, 2023, **127**, 9220–9228.

79 G. Herzberg, *Molecular Spectra and Molecular Structure. Spectra of Diatomic Molecules*, Krieger Publishing Company, Malabar, Florida, 1989, vol. 1.
80 D. B. Keck and C. D. Hause, *J. Mol. Spectrosc.*, 1968, **26**, 163–174.
81 X.-G. Zhang and P. B. Armentrout, *Eur. J. Mass Spectrom.*, 2004, **10**, 963–975.
82 M. Z. Martin, S. R. Desai, C. S. Feigerle and J. C. Miller, *J. Phys. Chem.*, 1996, **100**, 8170–8174.
83 S. C. Rasmussen, *ChemTexts*, 2015, **1**, 10.